LDA MEASUREMENTS OF TURBULENCE CHARACTERISTICS IN TRANSITION FROM RECTANGULAR TO COMPOUND UNSTEADY OPEN CHANNEL FLOWS

Iehisa Nezu
Department of Civil and Global Environment Engineering, Kyoto University
Kyoto, 606-8501, Japan
nezu@nezu.gee.kyoto-u.ac.jp

Michio Sanjou
Department of Civil and Global Environment Engineering, Kyoto University
Kyoto, 606-8501, Japan
sanjou@nezu.gee.kyoto-u.ac.jp

Yukiko Sakane
Department of Civil and Global Environment Engineering, Kyoto University
Kyoto, 606-8501, Japan
sakane@nezu.gee.kyoto-u.ac.jp

ABSTRACT

A time-dependent and depth-varying unsteady compound open-channel flow is one of the most important flows in hydraulic and river engineering. Therefore, the hydrodynamic characteristics of these flows should be investigated in detail. Recently, a lot of researches on unsteady rectangular open-channel flows were conducted intensively and consequently the important knowledge and database are now available. However, 3-D structure of unsteady compound open-channel flows is not available as yet. In particular, turbulent structure and secondary currents at the transition stage from the rectangular to compound channels have not been investigated, because it has been much difficult to measure them even with an LDA system. In this study, LDA measurements were conducted successfully in depth-varying unsteady compound open-channel flows with a channel transition process and 3-D turbulent structures were revealed experimentally.

INTRODUCTION

There are a lot of researches on compound open-channel flows that are composed of the main-channel and floodplains, because it is necessary in fundamental hydraulics and river engineering to investigate these flow structures and interactions in the view points of various hydraulic functions such as water discharge control, sediment transport and river environment. Early previous researches on compound open-channel flows have discussed mainly a flow interaction between main-channel and floodplains, e.g., Zheleznyakov(1985). With the development of innovative measurement systems, accurate turbulence measurements have been conducted in water flows. For example, Tominaga & Nezu(1991) have first measured turbulent structures in steady compound open-channel flows by using a laser Doppler anemometer(LDA) and revealed 3-D structure of primary flow and secondary currents. Ikeda *et al.*(1995) have measured secondary currents and horizontal vortices using LDA and a water-wave gauge. They have explained 3-D turbulent structure of compound open-channel experimentally. Sellin(1995) have investigated the friction law and 3-D velocity structure in a skewed two-stage flow with a large experimental flume. Nezu *et al.*(1999) have conducted LDA and PIV measurements, and found that the coherent structure observed in a platform eddy depends on the floodplain depth. On the other hand, there are also a lot of numerical simulations for compound open-channel flows. Naot *et al.*(1993) have calculated steady compound open-channel flows by using an algebraic stress model(ASM) and reproduced the main features in such compound channels. Nadaoka & Yagi(1998) and Bousmar & Zech(2001) have simulated a structure of platform vortices observed near the junction between the main-channel and floodplain by the use of a depth-averaged LES model, and discussed the stability of such a coherent structure numerically.

However, rivers in flood have often a depth-varying transition process from a rectangular to compound open-channel flows, and at such a transition stage the turbulent structure becomes more complicated due to an induced interaction between the main-channel and floodplains. Therefore, it is very important in river environment and for preventing water disaster to investigate these time-dependent and channel-changing hydrodynamics. In this study, 3-D LDA measurements were conducted in depth-varying unsteady free surface flows with a transition process from rectangular to compound channels, and 3-D turbulent structures in these transition flows were investigated experimentally.

Table 1: Hydraulic condition

case	H_b (cm)	H_p (cm)	B_f/B	H_b/D	Q_b (l/s)	Q_p (l/s)	Um_b (cm/s)	Um_p (cm/s)	T_d (s)	α ($\times 10^{-3}$)
TH60	4.0	8.3	0.5	0.8	2.3	13.8	28.8	59.4	60	1.62
TH120	4.0	8.0	0.5	0.8	2.3	13.8	28.8	62.7	120	0.72

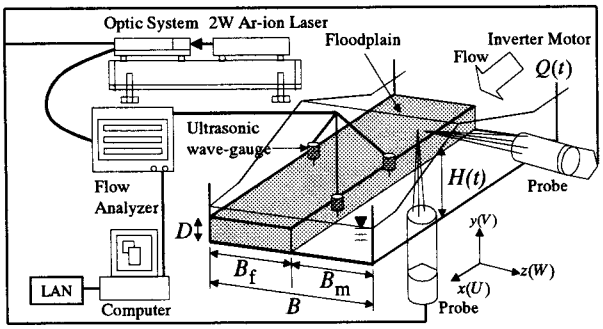

Fig.1: Experimental setup

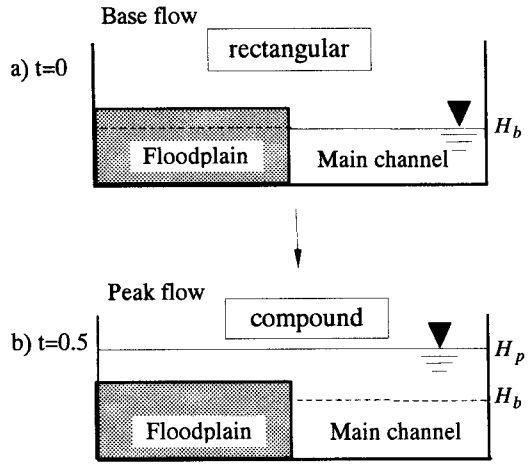

Fig.2: Unsteady open-channel flows with transition stage from rectangular to compound channels

EXPERIMENTAL SETUP AND HYDRAULIC CONDITIONS

Fig.1 shows the experimental setup. The turbulence measurements were conducted in a 10m long and 40cm wide tilting flume. The acrylic boxes were set on the right-hand side of the channel flume as a floodplain. In this figure, B is the channel width, B_f is the floodplain width, B_m is the main-channel width, H is the water depth in the main-channel, D is the height of floodplain. x is the streamwise coordinate, y and z are the vertical and spanwise ones. The ensemble-averaged velocity components in each direction are defined as U, V, W and the turbulence components are defined as u, v, w, respectively. The measuring zone is made of optical glass in all three walls of bottom and side walls, and thus the laser-beams can be projected into the channel water from both the side wall and the bottom as shown in Fig.1. In order to measure all three components of instantaneous velocities in the streamwise, vertical and spanwise directions, two sets of two component LDA probes (Dantec-made) were used. The discharge $Q(t)$ can be changed automatically by a controlled computer system with an electromagnetic flow-meter and an inverter motor. In this study, the discharge hydrograph was given by a triangle wave. These LDA probes were located at 7 m downstream from the channel entrance. For the simultaneous measurements of the time-dependent water depth $H(t)$, three sets of ultrasonic water-wave gauges were located above the main-channel and floodplain water surface. Table 1 indicates the hydraulic conditions. Two experimental cases were treated in this study. Both cases represent time-dependent unsteady free surface flows with the channel transition stage as shown in Fig.2. The base water depth at the time $t = 0$ was $H_b = 4$(cm) and the peak water depth $t = T_d$ was $H_p = 8$(cm). The corresponding base and peak discharges were $Q_b = 2.3$(l/s) and $Q_p = 13.8$(l/s), respectively. Two kinds of the duration time T_d of flood flow from the base depth to the peak depth were set as $T_d = 60$(s) and 120(s). The case names are called here as "TH60" and "TH120", respectively. α is the unsteadiness parameter of Nezu *et al.*(1997) and defined as

$$\alpha \equiv \frac{V_s}{U_c} \approx \frac{1}{(U_{mb}+U_{mp})/2}\frac{H_p - H_b}{T_d} \qquad (1).$$

EXPERIMENTAL RESULTS

Time-Variation of Primary Velocity and Water Depth

Fig.3 shows the time-variations of primary velocity $U(T)$ and water depth $H(T)$ at the center of main-channel ($z/B = 0.75$, $y/D = 0.54$) in the case of TH60. $T \equiv t/T_d$ is the normalized time by the duration time T_d. From this definition, $T = 0$ is the starting time of depth increasing and $T = 1.0$ is the peak-depth time. It is found that the primary velocity $U(T)$ attains a peak before the peak depth $T = 1.0$. Fig.4 is the relation of $U(T)$ and $H(T)$ at the same position as in Fig.3. Of particular significance is the counterclock-wise loops. It is well known that such flow loops are often observed in actual rivers in flood. It is recognized that the loop area is larger in TH60 (larger unsteadiness) than TH120 (small unsteadiness).

Fig.5 is the time-variations of water depth in the main-channel and floodplain. Of particular significance is that the water depth is larger in main-channel than on floodplain at the channel transition time ($0.2 < T < 0.6$). This hydrodynamic feature induces an important effect on secondary currents as will be mentioned later.

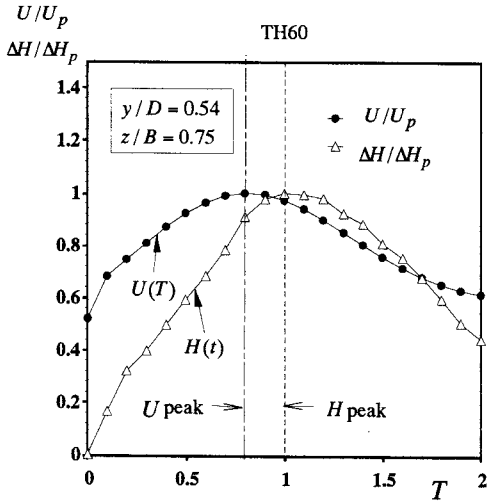

Fig.3: Time variations of mean velocity and water depth.

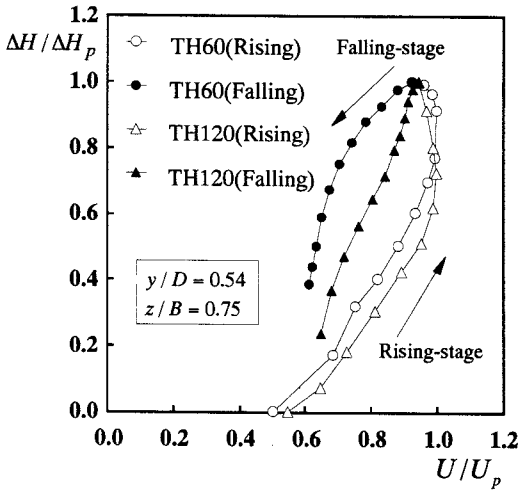

Fig.4 Loop property in unsteady open-channel flows

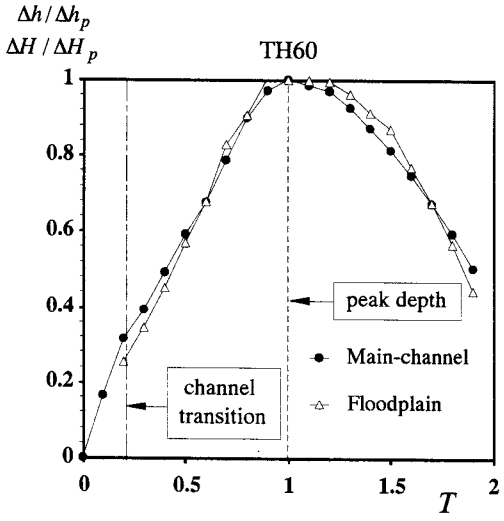

Fig.5 : Comparison of depth variations in main-channel and floodplain.

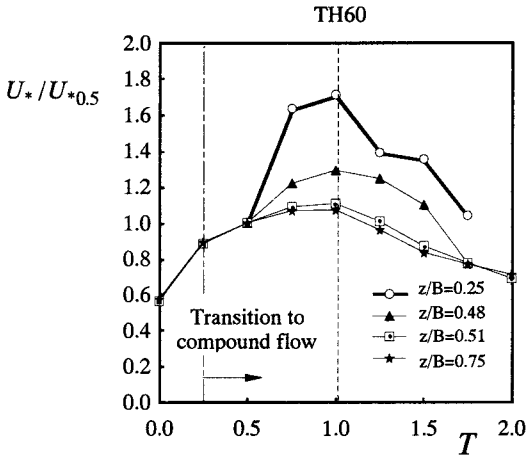

Fig.6: Time variations of friction velocity

Time-Variation of Friction Velocity

Fig.6 shows the time-variations of friction velocity U_* at $z/B = 0.25, 0.48, 0.51$ and 0.75. The local friction velocity U_* was calculated by the log-law that is described by

$$U/U_* = \frac{1}{\kappa}\ln(yU_*/\nu) + A \qquad (2)$$

in which, κ is the von Karman constant. In this study, the universal constant of $\kappa = 0.41$ was applied to the evaluation of friction velocity U_*. The friction velocity U_* normalized by $U_{*0.5}$ at $T = 0.5$ increases and decreases against the time T of flood. The time-variation of U_* is larger on the floodplain than in the main-channel. It should be noticed that the value of U_* on the floodplain $(z/B = 0.25)$ increases rapidly near the rising time-stage $(T = 0.5)$.

Secondary Flow in the Cross Section

Fig.7 shows the velocity vector description of the secondary currents (V,W) at the typical time phases in the case of TH60. The measured values are normalized by the maximum velocity U_{max} in the cross section. At the shallow stage $(T = 0.5)$, one-way secondary flow from the junction to floodplain is observed. It is considered that such a secondary flow is generated by the significant difference of water level between the main-channel and floodplain as shown in Fig.5. At the peak depth stage $(T = 1.0)$, typical secondary currents are generated from the junction edge toward the free surface. These features are almost same manner as observed in steady compound channels. At the falling stage $(T = 1.5)$, one-way secondary flow occurs on the floodplain. It should be noticed that such flows have the inverse directions to those in the rising stage $(T = 0.5)$. These time-dependent secondary flow plays an important role on mass transport and suspended sediment near the junction region in flooded rivers.

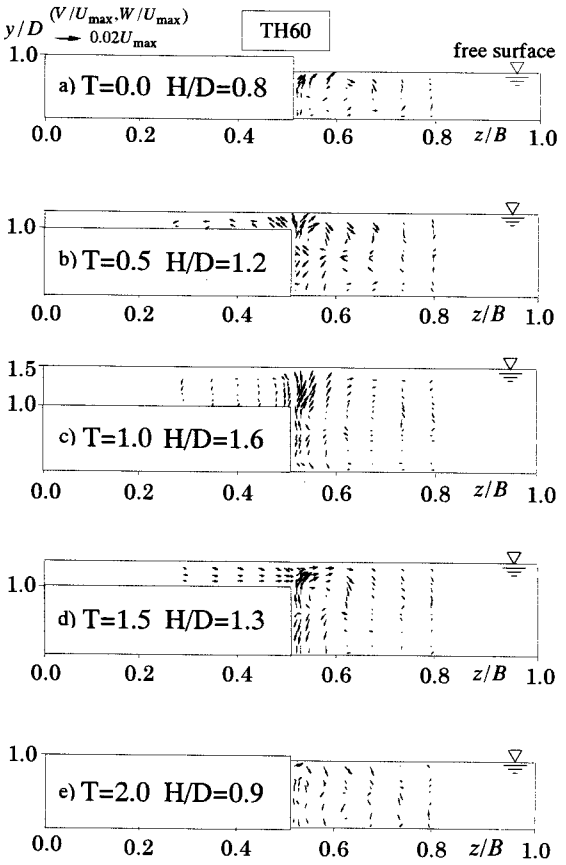

Fig.7 Variations of secondary flows (TH60)

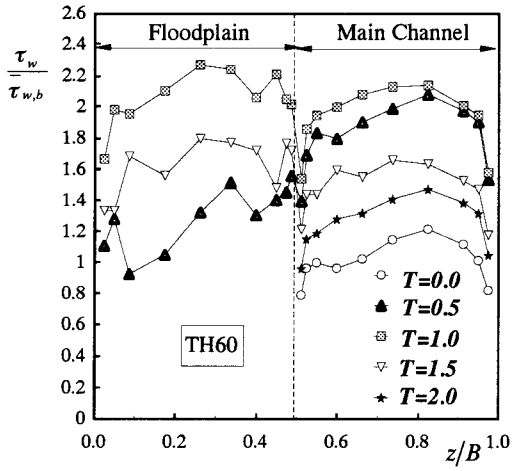

Fig.8: Distributions of wall shear stress(TH60)

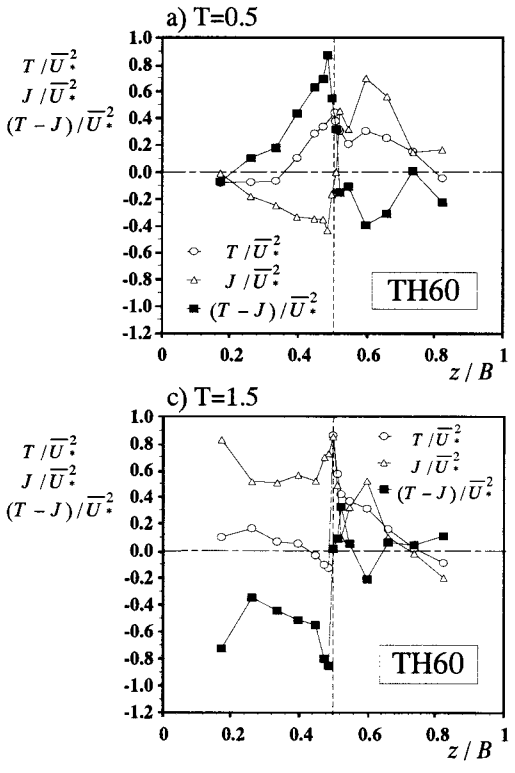

Fig.9: Structure of wall shear stress(TH60)

Spanwise Distributions of Wall Shear Stress

Fig.8 shows the distributions of wall shear stress $\tau_w \equiv \rho U_*^2$ as a function of time T. These results are normalized by the averaged value $\overline{\tau}_w$ along the perimeter. In all stages, the wall shear stress decreases locally near the junction edge. This feature is observed most remarkably at the peak depth of $T = 1.0$. It is also found that the differences of τ_w between the floodplain and main-channel decrease with an increase of the time-dependent flow depth $H(t)$.

The integration of the momentum equation from the wall ($y = 0$) to the free surface ($y = H$) leads to the following equation.

$$\frac{\tau_w}{\rho} = -\int_0^{h'} \frac{\partial U}{\partial t} dy + g I_e h' + \frac{d}{dz}(T - J)h' \qquad (3)$$

where,

$$T \equiv \frac{1}{h'}\int_0^{h'} (-\overline{uw}) dy \quad \text{and} \quad J \equiv \frac{1}{h'}\int_0^{h'} (UW) dy$$

It is understood from Eq.(3) that the spanwise Reynolds stress $-uw$ and the spanwise mean velocity W have a strong effect on the spanwise variations of the wall shear stress $\tau_w(z)$. Fig.9 shows the distributions of T, J and $(T-J)$ at the typical rising stage of $T = 0.5$ and the falling stage of $T = 1.5$. At the rising stage of $T = 0.5$, the one-way flow ($W < 0$) from the junction toward the floodplain occurs due to a flooded discharge. Therefore, the value of J becomes negative on floodplain, i.e., $z/B < 0.5$. In contrast, T increases from the floodplain to the junction, and consequently $d(T-J)/dz$ becomes positive. On the other hand, from the junction to main-channel, i.e., $z/B > 0.5$, $d(T-J)/dz$ becomes negative. This noticeable feature coincides well with the results of Fig.8. At the falling stage of $T = 1.5$, the one-way flow ($W > 0$) occurs from the floodplain to the junction and thus J becomes positive. J is larger than T on the floodplain and decides predominantly the distribution of $(T-J)$.

Primary Velocity in the Cross Section

Fig.10 shows the isovel lines of the primary flow normalized by the maximum velocity U_{max} in the case of TH60. The symbol x indicates the position of the appearance of U_{max}. At all typical time phases, velocity-dip phenomena are observed. In particular, this feature is the most remarkable at the peak depth time $T=1.0$. At the rising-transition stage($T=0.5$), the velocity of the main-channel is much larger than that over the floodplain. As the floodplain depth increases with time, the velocity differences between the main-channel and floodplain become smaller. Of particular significance is that the spanwise profiles of $U(z)$ decreases locally near the junction at $T=1.0$. This is because the secondary currents (see Fig.7) transport low-speed fluid toward the free-surface region. From these results, it is suggested strongly that there are significant differences of momentum and mass transport near the junction between the shallow-flow phase($T=0.5$) and deep-flow phase($T=1.0$).

Time-Dependent Properties of Reynolds Stress

Fig.11 shows the contour lines of the vertical Reynolds stress $-\overline{uv}$ against the time phase in the case of TH60. The value of $-\overline{uv}$ takes the positive and peak one near the channel bottom in all stages, which is called the "bottom shear stress". The negative distributions are observed near the main-channel junction. It is considered that this negative feature is connected to the fact that the velocity gradient $\partial U/\partial y$ becomes negative near the main-channel junction, which will be induced by secondary currents and velocity dip.

Fig.12 shows the contours of the spanwise Reynolds stress $-\overline{uw}$. In all compound channel stages, the value of $-\overline{uw}$ takes the negative one near the floodplain junction, whereas it takes the positive one near the main-channel junction. The isovel lines near the junction bulge from the junction edge toward the main-channel free surface. It is therefore considered that these features of $-\overline{uw}$ are caused by secondary currents of W.

Schematized Flow Modeling of the Depth-Varying Unsteady Compound Open-Channel Flows

Fig.13 shows the 3-D hydrodynamic characteristics in depth-varying unsteady free surface flows with a transition stage from rectangular to compound channels. Fig.13(a) shows the channel transition stage, in which the floodplain depth is very small and there are significant differences in primary velocity between the main-channel and floodplain. Ikeda *et al.*(1995) found that a single platform eddy is generated by shear instability in this stage. Furthermore, one-way flows occur from the junction toward floodplain region. It is therefore considered that such a secondary flow transports a lot of suspended sediments to floodplain at such shallow stage. Fig.13(b) is the rising depth stage. With an increase of water depth, secondary flow becomes stronger near the junction, and low momentum is transported up to the free surface region. Therefore, the

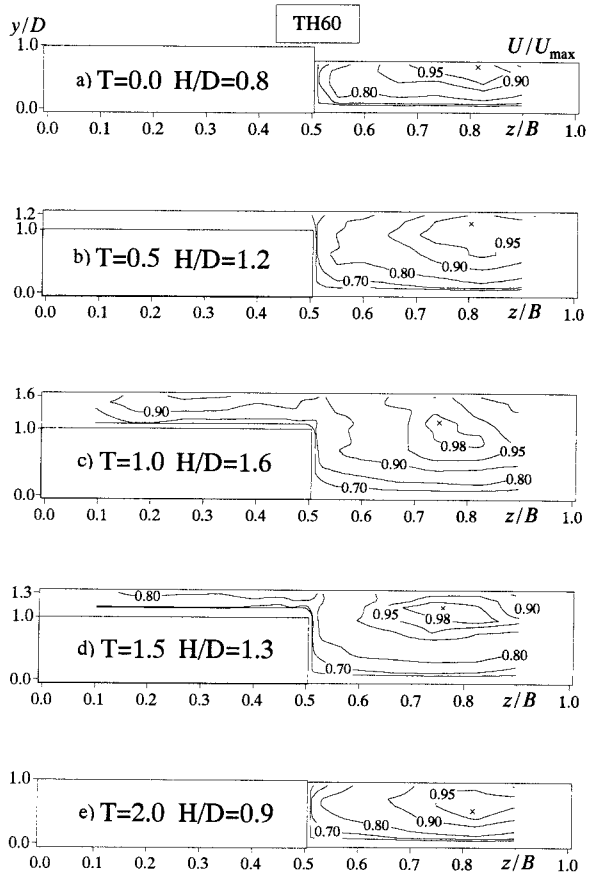

Fig.10: Primary velocity distributions (TH60)
(x means the position of maximum velocity)

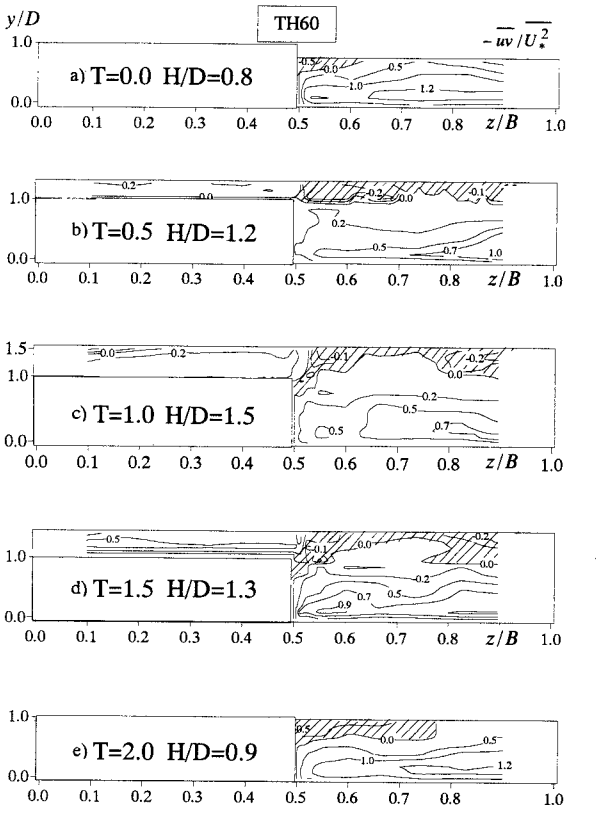

Fig.11: Distributions of vertical Reynolds stress $-\overline{uv}$ (TH60)

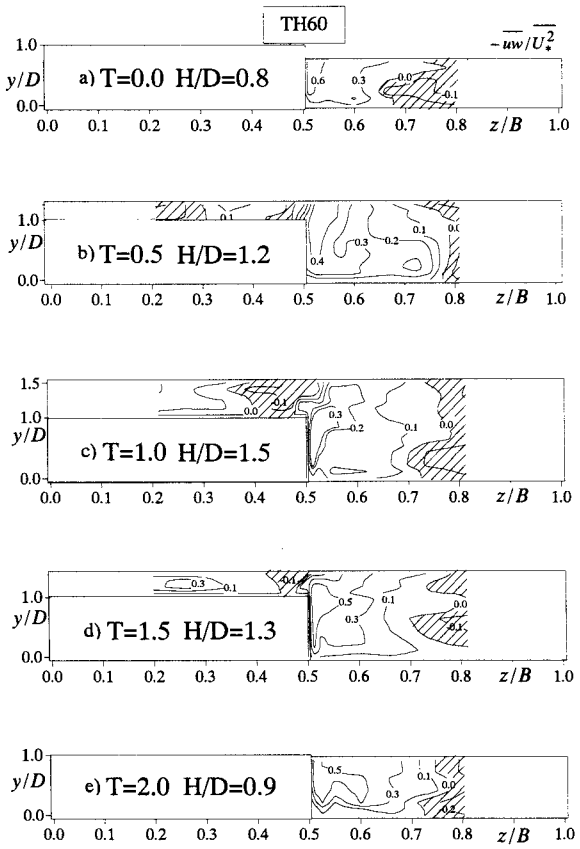

Fig.12: Distributions of spanwise Reynolds stress $-\overline{uw}$ (TH60)

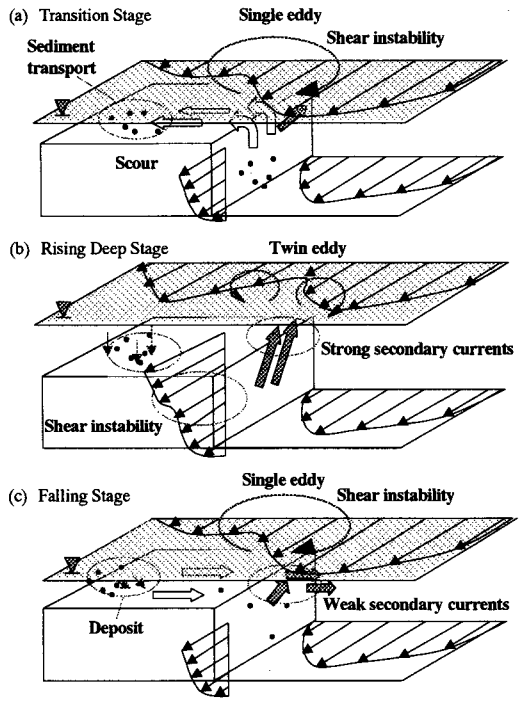

Fig.13: Schematized hydrodynamic structures in unsteady compound open-channel flow.

distribution of primary velocity $U(z)$ decreases locally near the junction region and consequently two inflectional points are formed as described in Fig.13(b). Nezu et al. (1999) found that twin coherent eddies are generated due to two-point inflectional structures.

Fig.13(c) is the falling depth stage. With a decrease of water depth, the velocity distribution $U(z)$ returns to the same structure as the shallow water stage. In this stage, one-way flows are generated from the floodplain toward the junction.

CONCLUSIONS

In this study, 3-D turbulence measurements were conducted in unsteady open-channel flows with a transition stage from rectangular to compound channels. The unsteadiness properties of primary velocity, secondary currents and turbulence were revealed experimentally. The main findings in this study are as follows:

1. The time-variation of friction velocity is larger on the floodplain than in the main-channel. The value of friction velocity on the floodplain increases rapidly near the transition-time stage.
2. At the channel transition stage, in which the floodplain depth is very small, one-way secondary flow is generated on floodplain. These flows play an important role on sediment transports. At the peak depth, there is a typical structure of secondary currents, which is almost same manner as that of a steady flow.
3. The distributions of primary velocity and Reynolds stress depend on the water depth and secondary currents. It should be noticed that primary velocity profiles in the spanwise direction vary largely with time, in the connection with single and twin horizontal eddies.

References

Bousmar, D. and Zech, Y., 2001, "Periodic turbulent structures modeling in a symmetric compound channel", *Proc. of 29th IAHR Corgress,* Beijing, pp.244-249.

Ikeda, S., Murayama, N. and Kuga, T., 1995, " Stability of horizontal vortices in compound open channel flow and their 3-D structure", *J. of Hydraulic, Coastal and Envir. Eng.*, JSCE, No.509/ II -30, pp.131-142. (in Japanese)

Nadaoka, K. and Yagi, H., 1998, "Shallow-water turbulence modeling and horizontal large eddy computation of river flow", *J. of Hydraulic Eng.*, ASCE, Vol.124, No.5, pp.493-500.

Naot, D., Nezu, I. and Nakagawa, H., 1993, "Hydrodynamic behavior of compound rectangular open-channel flows", *J. of Hydraulic Eng.*, ASCE, vol.119, pp.390-408.

Nezu, I., Kadota, A. and Nakagawa, H., 1997, "Turbulent structure in unsteady depth-varying open-channel Flows", *J. of Hydraulic Eng.*, ASCE, Vol.123, pp.752-763.

Nezu, I., Onitsuka, K. and Iketani, K., 1999, "Coherent horizontal vortices in compound open-channel flows", *HYDRAULIC MODELING*(ed. Singh et al.), Water Resources Pub., Colorado, pp.17-32.

Sellin, B.H.J., 1995, "Hydraulic performance of a skewed two-stage flood channel", *J. of Hydraulic Res.*, IAHR, Vol.33, No.1, pp.43-64.

Tominaga, A. and Nezu, I., 1991, "Turbulent structure in compound open channel flows", *J. of Hydraulic Eng.*, ASCE, Vol.117, pp.21-41.

Zheleznyakov, G.E., 1985, "Problem of the interaction of the main channel and the flood plain flows", *Proc. of 21st IAHR Congress,* Melbourne, Vol.3, pp.372-376.